JOURNAL

OF THE AMERICAN CHEMICAL SOCIETY

VOLUME 105, NUMBER 12 JUNE 15, 1983

Molybdenum K-Edge Extended X-ray Absorption Fine Structure (EXAFS) Studies of Synthetic Mo–Fe–S Clusters Containing the MoS_4 Unit: Development of a Fine Adjustment Technique Based on Models

Boon-Keng Teo,*[†] Mark R. Antonio,[‡] and Bruce A. Averill*[‡]

Contribution from Bell Laboratories, Murray Hill, New Jersey 07974, and Department of Chemistry, Michigan State University, East Lansing, Michigan 48824. *Received June 14, 1982*

Abstract: The Mo K-edge extended X-ray absorption fine structure (EXAFS) spectra of the binuclear dianionic complexes $[S_2MoS_2FeL_2]^{2-}$ (**1**, L = SPh; **2**, L = Cl; **3**, L = OPh; Et_4N^+ salts), the trinuclear complexes $[S_2MoS_2FeS_2Fe(S\text{-}p\text{-}CH_3C_6H_4)_2]^{3-}$ (**4**, Et_4N^+ salt), $[S_2MoS_2FeS_2MoS_2]^{3-}$ (**5**, Et_4N^+ salt) and $[Cl_2FeS_2MoS_2FeCl_2]^{2-}$ (**6**, Ph_4P^+ salt), as well as the NH_4^+ salt of $[MoS_4]^{2-}$ (**7**), have been measured in the transmission mode. Data analysis using theoretical amplitude and phase functions provided better than 1 and 2% accuracy for the Mo–S and Mo–Fe distances, respectively. To improve the accuracy as well as to provide a reliable measure of the number of neighbors, a technique for fine adjustment based on models (FABM) was developed. The FABM technique relies upon a detailed exploration of the multidimensional parameter correlation space in the curve fitting, from which a simple method has been devised to alleviate parameter correlation problems. With the FABM technique, interatomic distances and coordination numbers can be determined to better than 0.5 and 10% and 1 and 20% accuracy for the major (Mo–S) and the minor (Mo–Fe) terms, respectively. In addition, the FABM technique enables one to discover and discriminate against local minima in the curve fitting and, most importantly, to distinguish a good model compound from a bad one. The criterion for a good model compound is that the multidimensional χ^2 minimum surface in the parameter correlation space must have *parameters* and *curvature* similar to those of the unknown. (The criterion is also applicable to other curve-fitting techniques.) While it is almost impossible to explore all the parameters, we have focused our attention on the correlations of the few most important ones (ΔE_0^p vs. Δr, and B vs. σ). The FABM method is distinct from other model-dependent techniques in that only one parameter (ΔE_0^*), *and not the total phase function*, needs to be obtained from the model to calculate the distance in the unknown. Similarly, only two parameters (σ^*, S^*), *and not the complete backscattering function*, need to be obtained from the model to calculate the number of neighbors in the unknown. In the FABM approach, theoretical phase and amplitude functions, rather than functions extracted from models, are used in the curve fitting. In this respect, the method is less critically dependent on the models than other model-based techniques. Finally, terminal and bridging Mo–S distances for **1–5** can also be determined quite accurately from the average Mo–S distance and the distance spread estimated from the Debye–Waller factor as determined by EXAFS. The EXAFS technique also allows accurate determination of metal–ligand distances in $[S_2MoS_2FeCl_2]^{2-}$, for which a twofold static disorder results only in average distances being obtainable from single-crystal X-ray crystallography.

Introduction

Extended X-ray absorption fine structure (EXAFS) spectroscopy has gained wide recognition as a powerful structural technique with applications to many important chemical[1] and biochemical[2] systems. It has proven especially useful for probing the immediate environment around a selected X-ray-absorbing atom in large and complex biological molecules. For example, the molybdenum sites in the MoFe protein[3a,b] and both the molybdenum[3b] and iron[4] sites in the iron–molybdenum cofactor isolated from the MoFe protein of the enzyme nitrogenase have been studied by EXAFS spectroscopy. The EXAFS results have been interpreted as indicating that the molybdenum has four or

[†] Bell Laboratories.

[‡] Michigan State University. Current addresses: M.R.A., The Standard Oil Co. (Ohio), Cleveland, Ohio 44128; B.A.A., Department of Chemistry, University of Virginia, Charlottesville, Virginia 22901.

(1) (a) Stern, E. A. *Contemp. Phys.* **1978**, *19*, 289. (b) Lee, P. A.; Citrin, P. H.; Eisenberger, P.; Kincaid, B. M. *Rev. Mod. Phys.* **1981**, *53*, 769. (c) Eisenberger, P.; Kincaid, B. M. *Science*, **1978**, *200*, 1441. (d) Sandstrom, D. R.; Lytle, F. W. *Annu. Rev. Phys. Chem.* **1979**, *30*, 215. (e) Teo, B. K. *Acc. Chem. Res.* **1980**, *13*, 412. (f) Teo, B.-K. In "EXAFS Spectroscopy: Techniques and Applications"; Teo, B.-K., Joy, D. C., Eds.; Plenum Press: New York, 1981; pp 13–58.

(2) (a) Shulman, R. G.; Eisenberger, P.; Kincaid, B. M. *Annu. Rev. Biophys. Bioeng.* **1978**, *7*, 559. (b) Cramer, S. P.; Hodgson, K. O. *Prog. Inorg. Chem.* **1979**, *25*, 1. (c) Doniach, S.; Eisenberger, P.; Hodgson, K. O. In "Synchrotron Radiation Research"; Winick, H., Doniach, S., Eds.; Plenum Press: New York, 1980; pp 425–458. (d) Chan, S. I.; Gamble, R. C. *Methods Enzymol.* **1978**, *54E*, 323. (e) Powers, L. S. *Biochim. Biophys. Acta Rev.: Bioenerg.* **1982**, 683, 1.

0002-7863/83/1505-3751$01.50/0

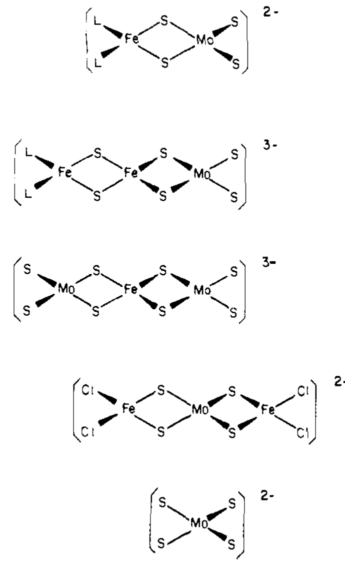

1, L=SPh
2, L=Cl
3, L=OPh
4, L=S-p-Tolyl
5
6
7

Figure 1. Schematic of the structures of the Mo–Fe–S compounds **1–7** containing the MoS_4 unit.

five sulfur atoms and either two[3a,5] or three[3a–c] iron atoms as nearest neighbors, and that the iron atoms have an average of approximately 3.4 ± 1.6 sulfur (or chlorine), 2.3 ± 0.9 iron, 0.4 ± 0.1 molybdenum, and 1.2 ± 1.0 oxygen (or nitrogen) atom(s) as nearest neighbors.[4] These EXAFS results, together with chemical analyses and spectroscopic properties, suggest that the FeMo cofactor of nitrogenase contains a novel Mo–Fe–S cluster[6–8] with possible oxygen (or nitrogen) ligation to iron.[9,10] We report herein the determination of interatomic distances, Debye–Waller factors, and coordination numbers from the Mo K-edge EXAFS measurements for an extensive series of Mo–Fe–S clusters containing the MoS_4 moiety (Figure 1). This series of Mo–Fe–S clusters is of particular importance[11] both for their possible relevance as structural fragments of the FeMo cofactor and as models for EXAFS studies of other biological or synthetic systems containing Mo–Fe–S constituents.

In this paper, we focus our attention on the development of a reliable and accurate data analysis technique that improves the accuracy of the distances and numbers of neighbors provided by EXAFS. In addition, the method provides a means of distinguishing a good model compound from a bad one for a particular unknown system, based on a detailed analysis of the multidimensional parameter correlations. Specifically, the method involves curve fitting the unknown and model spectra with the generally accepted phenomenological EXAFS equation based on short-range single-scattering theory,[12–16] using the ab initio

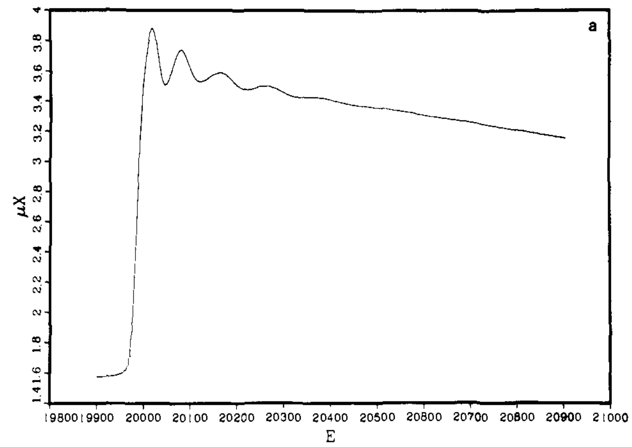

Figure 2. Molybdenum K-edge X-ray absorption spectrum, μX vs. E (eV), of (a) $[S_2MoS_2Fe(SPh)_2]^{2-}$ (**1**). The corresponding data for compounds **2–7** are presented in Figures 2b–g, respectively, included as supplementary material.

backscattering amplitude and phase functions of Teo and Lee.[17] We shall refer to this as "best fit based on theory" (BFBT). The parameter correlations often encountered in the curve fitting, which can affect the accuracy, are subsequently quantified to yield phase and amplitude *correlation curves* for each term in the EXAFS equation. These curves are characteristic of the type of compounds and hence carry chemical information not available by best fitting alone. Using these parameter correlation curves, we have developed a set of simple criteria that enables us to distinguish a good model compound from a bad one. (Note that these criteria are also applicable to other curve-fitting techniques.) With a good model, these curves can be used to improve the accuracy of the EXAFS structural determination. This "fine adjustment based on model" compounds technique will be referred to as FABM. The FABM method is distinct from other model-dependent techniques in that only one parameter (ΔE_0^*), *and not the total phase function*, needs to be obtained from the model to calculate the distance in the unknown. Similarly, only two parameters (σ^*, S^*), *and not the complete backscattering function*, need to be obtained from the model to calculate the number of neighbors in the unknown. In the FABM approach, theoretical phase and amplitude functions, rather than functions extracted from models, are used in the curve fitting. In this respect, the method is less critically dependent on the models than other model-based techniques. Finally, we will also show that terminal and bridging Mo–S distances in these compounds can be determined to a high degree of accuracy with the aid of the EXAFS-determined Debye–Waller factor for small differences in bond lengths (≲0.1 Å).

Experimental Section

Materials. The binuclear dianionic complexes $[S_2MoS_2FeL_2]^{2-}$ (**1**, L = SPh;[18a,19a] **2**, L = Cl;[18a,20a,b] **3**, L = OPh;[18b,c] Et_4N^+ salts) and the trinuclear trianionic complex $[S_2MoS_2FeS_2Fe(S\text{-}p\text{-}CH_3C_6H_4)_2]^{3-}$ [18c,d] (**4**, Et_4N^+ salt) were prepared according to the methods given by Averill et

(3) (a) Cramer, S. P.; Hodgson, K. O.; Gillum, W. O.; Mortenson, L. E. *J. Am. Chem. Soc.* **1978**, *100*, 3398. (b) Cramer, S. P.; Gillum, W. O.; Hodgson, K. O.; Mortenson, L. E.; Stiefel, E. I.; Chisnell, J. R.; Brill, W. J.; Shah, V. K. *Ibid.* **1978**, *100*, 3814. (c) Wolff, T. E.; Berg, J. M.; Warrick, C.; Hodgson, K. O.; Holm, R. H. *Ibid.* **1978**, *100*, 4630.

(4) Antonio, M. R.; Teo, B.-K.; Orme-Johnson, W. H.; Nelson, M. J.; Groh, S. E.; Lindahl, P. A..; Kauzlarich, S. M.; Averill, B. A. *J. Am. Chem. Soc.* **1982**, *104*, 4703.

(5) Teo, B.-K.; Averill, B. A. *Biochem. Biophys. Res. Commun.* **1979**, *88*, 1454.

(6) Shah, V. K.; Brill, W. J. *Proc. Natl. Acad. Sci. U.S.A.* **1977**, *74*, 3249.

(7) Burgess, B. K.; Jacobs, D. B.; Stiefel, E. I. *Biochim. Biophys. Acta* **1980**, *614*, 196.

(8) Rawlings, J.; Shah, V. K.; Chisnell, J. R.; Brill, W. J.; Zimmermann, R.; Münck, E.; Orme-Johnson, W. H. *J. Biol. Chem.* **1978**, *253*, 1001.

(9) Smith, B. E. In "Molybdenum Chemistry of Biological Significance", Newton, W. E., Otsuka, S., Eds.; Plenum, Press: New York, 1980; pp 179–190.

(10) Newton, W. E.; Burgess, B. K.; Stiefel, E. I. In ref 9, pp 191–202.

(11) (a) Averill, B. A. *Struct. Bonding (Berlin)* **1983**, *53*, 59. (b) Coucouvanis, D. *Acc. Chem. Res.* **1981**, *14*, 201.

(12) (a) Sayers, D. E.; Lytle, F. W.; Stern, E. A. *Adv. X-Ray Anal.* **1970**, *13*, 248–271. (b) Sayers, D. E.; Stern, E. A.; Lytle, F. W. *Phys. Rev. Lett.* **1971**, *27*, 1204. (c) Lytle, F. W.; Sayers, D. E.; Stern, E. A. *Phys. Rev. B* **1975**, *11*, 4825. (d) Stern, E. A.; Sayers, D. E.; Lytle, F. W. *Ibid.* **1975**, *11*, 4836, and references cited therein.

(13) Stern, E. A. *Phys. Rev. B* **1974**, *10*, 3027.

(14) Ashley, C. A.; Doniach, S. *Phys. Rev. B* **1975**, *11*, 1279.

(15) (a) Lee, P. A.; Pendry, J. B. *Phys. Rev. B* **1975**, *11*, 2795. (b) Lee, P. A.; Beni, G. *Ibid.* **1977**, *15*, 2862.

(16) Kincaid, B. M.; Eisenberger, P. *Phys. Rev. Lett.* **1975**, *34*, 1361.

(17) Teo, B.-K.; Lee, P. A. *J. Am. Chem. Soc.* **1979**, *101*, 2815.

(18) (a) Tieckelmann, R. H.; Silvis, H. C.; Kent, T. A.; Huynh, B. H.; Waszczak, J. V.; Teo, B.-K.; Averill, B. A. *J. Am. Chem. Soc.* **1980**, *102*, 5550. (b) Silvis, H. C.; Averill, B. A. *Inorg. Chim. Acta* **1981**, *54*, L57. (c) Teo, B.-K.; Antonio, M. R.; Tieckelmann, R. H.; Silvis, H. C.; Averill, B. A. *J. Am. Chem. Soc.*, **1982**, *104*, 6126. (d) Tieckelmann, R. H.; Averill, B. A. *Inorg. Chim. Acta* **1980**, *46*, L35.

(19) (a) Coucouvanis, D.; Simhon, E. D.; Swenson, D.; Baenziger, N. C. *J. Chem. Soc., Chem. Commun.* **1979**, 361. (b) Coucouvanis, D.; Simhon, E. D.; Baenziger, N. C. *J. Am. Chem. Soc.* **1980**, *102*, 6644. (c) Coucouvanis, D.; Baenziger, N. C.; Simhon, E. D.; Stremple, P.; Swenson, D.; Simopoulous, A.; Kostikas, A.; Petrouleas, V.; Papaefthymiou, V. *Ibid.* **1980**, *102*, 1732.

(20) (a) Müller, A.; Tülle, M. G.; Bögge, H. *Z. Anorg. Allg. Chem.* **1980**, *471*, 115. (b) Müller, A.; Jostes, R.; Tülle, M. G.; Trautwein, A.; Bill, E. *Inorg. Chim. Acta* **1980**, *46*, L121. (c) Müller, A.; Sarkar, A.; Dommröse, A. M.; Filgueira, R. *Z. Naturforsch. Teil B* **1980**, *35*, 1592.

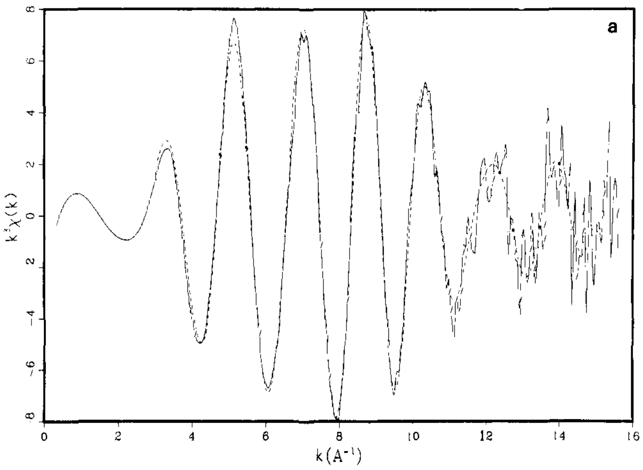

Figure 3. Background-subtracted (solid curve) and Fourier-filtered (dashed curve) $k^3\chi(k)$ (Å^{-3}) vs. k (Å^{-1}) EXAFS data for **1** (a). Data for compounds **2–7** are presented in Figures 3b–g, respectively, included as supplementary material.

al.[18] The trinuclear complexes $[S_2MoS_2FeS_2MoS_2]^{3-}$[19b,21] (**5**, Et_4N^+ salt) and $[Cl_2FeS_2MoS_2FeCl_2]^{2-}$[19c,20c] (**6**, Ph_4P^+ salt) were prepared following the procedures given by Coucouvanis et al.[19] The NH_4^+ salt of $[MoS_4]^{2-}$ (**7**) was prepared according to a literature method.[22]

The experiments were performed on pressed boron nitride pellet samples. The sample cells ((1–3) × 3 × 19 mm^3) were sealed with 1-mil Kapton tape.

X-ray Absorption Measurements. The X-ray absorption measurements were performed at the Cornell High Energy Synchrotron Source (CHESS) on the C2 EXAFS beam line using the synchrotron radiation from the Cornell Electron Storage Ring (CESR) at the Wilson Laboratory of Cornell University.[23]

The molybdenum K-edge EXAFS spectra of the compounds were taken with the transmission technique at ambient temperature,[24] using a channel-cut silicon ⟨220⟩ crystal monochromator that was detuned by ~50% for harmonic rejection.[25]

Data Analysis

Data Reduction. The raw data were accumulated as a function of photon energy E in such a way as to produce uniformly spaced intervals in k space (vide infra). Figure 2a shows a typical plot of $\mu X = \ln (I_0/I)$ vs. E at and above the molybdenum K-edge of $[S_2MoS_2Fe(SPh)_2]^{2-}$ (**1**). For EXAFS analysis, it is necessary to convert the photon energy E into photoelectron wave vector $k = [2m/\hbar^2 (E - E_0)]^{1/2}$, where E_0 is the energy threshold of the molybdenum K-edge and m is the mass of an electron. After conversion to k space in which E_0 was chosen at 19 980 eV, the data were multiplied by k^3 and the background was removed (five sections of ca. 3 Å^{-1} each) by using a cubic spline technique.[1b,26a] The resulting modulation of the absorption coefficient, the EXAFS $\chi(k)$, in the form $k^3\chi(k)$ vs. k, was normalized by dividing by the edge jump and corrected for the absorption dropoff via Victoreen's true absorption equation.[27] Typical $k^3\chi(k)$ vs. k data are shown as a solid curve in Figure 3a for **1**. For the purpose of curve fitting, the high-frequency noise and the small residual background in each spectrum were removed by a Fourier filtering (window: 0.8–4.2 Å) technique.[1b,26b] The resulting filtered data (dashed curve), subsequently truncated at 3 and 14.5 Å^{-1}, are compared with the unfiltered data in Figure 3a for **1**. The corresponding Fourier transforms of the unfiltered, untruncated EXAFS data are depicted in Figures 4a, 4f, and 4g for **1**, **6**, and **7**, respectively. The Fourier transforms for **2–5** are available as Supplementary Material (Figure 4, b–e). Data filtered in this way were used in the following curve-fitting procedure.

Best Fit Based on Theory (BFBT). A nonlinear least-squares program, which utilizes Marquardt's scheme,[28] was used in the curve fitting. For the present systems which contain two different types of nearest neighbors, a two-term fit of the following expression was used:[29]

$$k^3\chi(k) = B_S F_S(k_S) k_S^2 e^{-2\sigma_S^2 k_S^2} \frac{\sin\,[2k_S r_S + \phi_S(k_S)]}{r_S^2} + B_{Fe} F_{Fe}(k_{Fe}) k_{Fe}^2 e^{-2\sigma_{Fe}^2 k_{Fe}^2} \frac{\sin\,[2k_{Fe} r_{Fe} + \phi_{Fe}(k_{Fe})]}{r_{Fe}^2} \quad (1)$$

The terms $F_j(k_j)$, $\phi_j(k_j)$, σ_j, r_j, and k_j denote the amplitude, the phase, the Debye–Waller factor, the interatomic distance, and the photoelectron wave vector, respectively, for the jth type of neighboring atom where j = S, Fe. For the K-edge of molybdenum, the phase functions are: $\phi_S = \phi_{Mo}{}^a + \phi_S{}^b - \pi$ for Mo–S and $\phi_{Fe} = \phi_{Mo}{}^a + \phi_{Fe}{}^b - \pi$ for Mo–Fe where $\phi_{Mo}{}^a$ is the absorber (Mo) phase function and $\phi_S{}^b$ and $\phi_{Fe}{}^b$ are backscattering phase functions due to S and Fe, respectively. The factor of π is included to take care of an overall minus sign (for K-edge EXAFS only). The amplitude $F(k)$ and the phase $\phi(k)$ functions employed were the theoretical curves calculated by Teo and Lee.[17] For each k_j value, $F_j(k_j)$ and $\phi_j(k_j)$ were interpolated from the theoretical values.[30]

The scale factor B_j can be related to the number of bonds N_j of the jth type of neighboring atoms (j = S, Fe) and the amplitude reduction factor, S_j, as follows:

$$B_j = N_j S_j \quad (2)$$

Strictly speaking, the amplitude reduction factor S_j has a k dependence[31,32] and is related to the lifetime of the core hole,[33] inelastic losses at the absorbing atom, $s_0^2(k)$, which are due both to many-body effects such as shake-up/shake-off processes, and scattering by neighboring atoms j and the medium inbetween,[32b] $e^{-2r_j/\lambda(k)}$ (where $\lambda(k)$ is the inelastic electron mean free path):

$$S_j(k) = s_0^2(k) e^{-2r_j/\lambda(k)} \quad (3)$$

Since $s_0^2(k)$ tends to reduce the EXAFS amplitude at high k, whereas $e^{-2r_j/\lambda(k)}$, because of the k dependence of $\lambda(k)$, tends to attenuate more amplitude at low k, we approximate $S_j(k)$ by the scalar S_j which may vary from shell to shell.[34] It is obvious from

(21) McDonald, J. W.; Friesen, G. D.; Newton, W. E. *Inorg. Chim. Acta* **1980**, *46*, L79.

(22) Krüss, G. *Justus Liebigs Ann. Chem.* **1884**, *225*, 1.

(23) Batterman, B. W. In ref 1f, pp 197–204.

(24) (a) Typical storage ring parameters were: energy, 5.18 GeV; current 4–12 mA; bend radius at synchrotron light ports, 32 m; horizontal range of synchrotron radiation at the beam line, 14 mrad. (b) Beam size: 1 × 12 mm. Incident (I_0) and transmitted (I) beam intensities were measured by ionization chambers of 8 and 30 cm in length and filled with argon (flow type). (c) The EXAFS spectra were typically recorded with an integration time of 1–2 s/point (constant I_0 accumulation) with 150 steps covering about 900 eV above the Mo K-edge (19 900 to 20 900 eV). The data were taken in constant k steps, which amounted to 3 eV/point at the beginning and 10 eV/point at the end of the scan. We note that the energy resolution at 20 keV for a beam height of 1 mm at the 13.6 m point (C2 line) is ca. 9 eV.

(25) Mills, D.; Pollock, V. *Rev. Sci. Instrum.* **1980**, *51*, 1664.

(26) (a) A local cubic spline background removal program. Spline approximation algorithm form: Fox, P. A.; Hall, A. D.; Schryer, N. L. The PORT Mathematical Subroutine Library, **1976**, Bell Laboratories Computing Science Technical Report No. 47. (b) Local Fourier transform and filtering routines developed by B. M. Kincaid, Bell Laboratories.

(27) "International Tables for X-Ray Crystallography", Macgillavry, C. H., Rieck, G. D., Lonsdale, K., Eds.; Kynoch Press: Birmingham, England, 1968; Vol. III, pp 171–173. The correction was applied according to $\mu_0/\rho = C\lambda^3 - D\lambda^4$ with C = 555 and D = 296 for molybdenum.

(28) Marquardt, D. W. *J. Soc. Ind. Appl. Math.* **1963**, *11*, 431.

(29) (a) Teo, B.-K.; Shulman, R. G.; Brown, G. S.; Meixner, A. E. *J. Am. Chem. Soc.* **1979**, *101*, 5624. (b) Teo, B.-K.; Eisenberger, P., Kincaid, B. M. *Ibid.* **1977**, *100*, 1735.

(30) The theoretical EXAFS functions employed herein were obtained in ref 17 from Table VII for the central atom phase ϕ^a_{Mo} (calculated using the Herman–Skillman wave function), from Table II for the backscattering phases ϕ^b_S, ϕ^b_{Fe} (calculated using Clementi–Roetti wave functions), and from Table I for the backscattering amplitudes F_S, F_{Fe} (calculated using Clementi–Roetti wave functions).

(31) The amplitude reduction factors are due to a combination of many-electron effects[32,33] (including core-relaxation effects and inelastic processes originating within the central atom), the energy resolution of the monochromator,[36a] and to thickness effects.[42]

(32) (a) Stern, E. A.; Heald, S. M.; Bunker, B. *Phys. Rev. Lett.* **1979**, *42*, 1372. (b) Stern, E. A.; Bunker, B. A.; Heald, S. M. *Phys. Rev. B* **1980**, *21*, 5521.

(33) Ekardt, W.; Thoai, D. B. T. *Solid State Commun.* **1981**, *40*, 939.

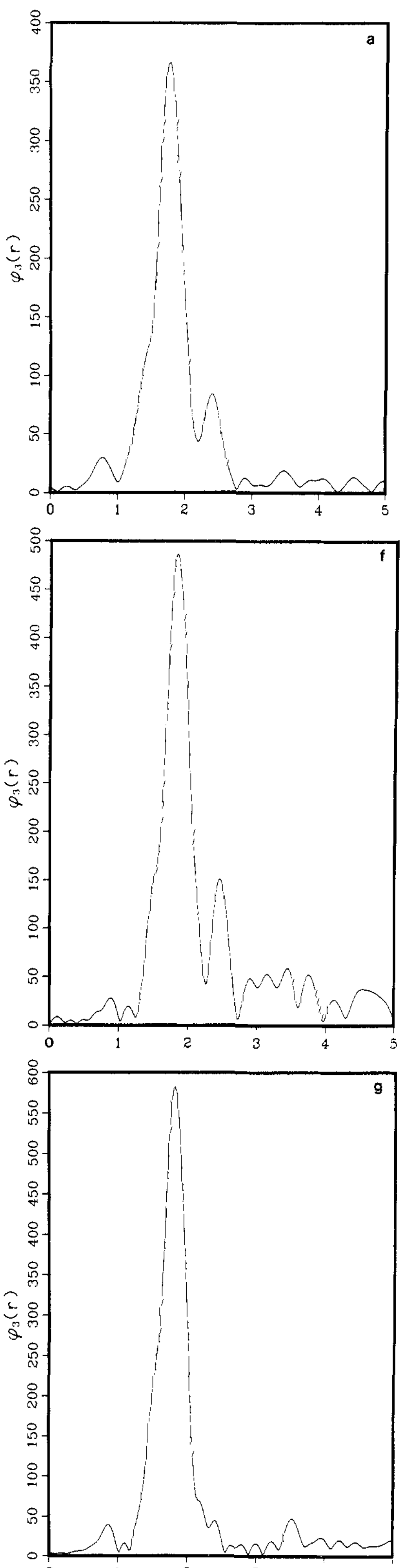

Figure 4. Fourier transforms $\varphi_3(r)$ vs. r (Å) (before phase shift correction) of the background-subtracted $k^3\chi(k)$ vs. k EXAFS spectra (solid curves in Figure 3) for **1** (a), **6** (f), **7** (g). See supplementary material for Fourier transforms of **2**–**5**.

eq 2 that if we know the amplitude reduction factor S_j we can calculate the number of bonds N_j from the fitted scale factor B_j.

Eight parameters are varied in the nonlinear least-squares curve fitting: the two scale factors B_S and B_{Fe}, two Debye-Waller factors σ_S and σ_{Fe}, two distances r_S and r_{Fe}, and two threshold energy differences ΔE_{0_S} and $\Delta E_{0_{Fe}}$. Figures 5a, 5f, and 5g show the best fits (dashed curves) of this EXAFS model to the Fourier-filtered data (solid curves) of **1**, **6**, and **7**. The corresponding data for **2**–**5** are included as Supplementary Material (Figures 5b–e). For a single-term fit, such as with MoS_4^{2-}, only four parameters (B_S, σ_S, r_S, and ΔE_{0_S}) are refined.

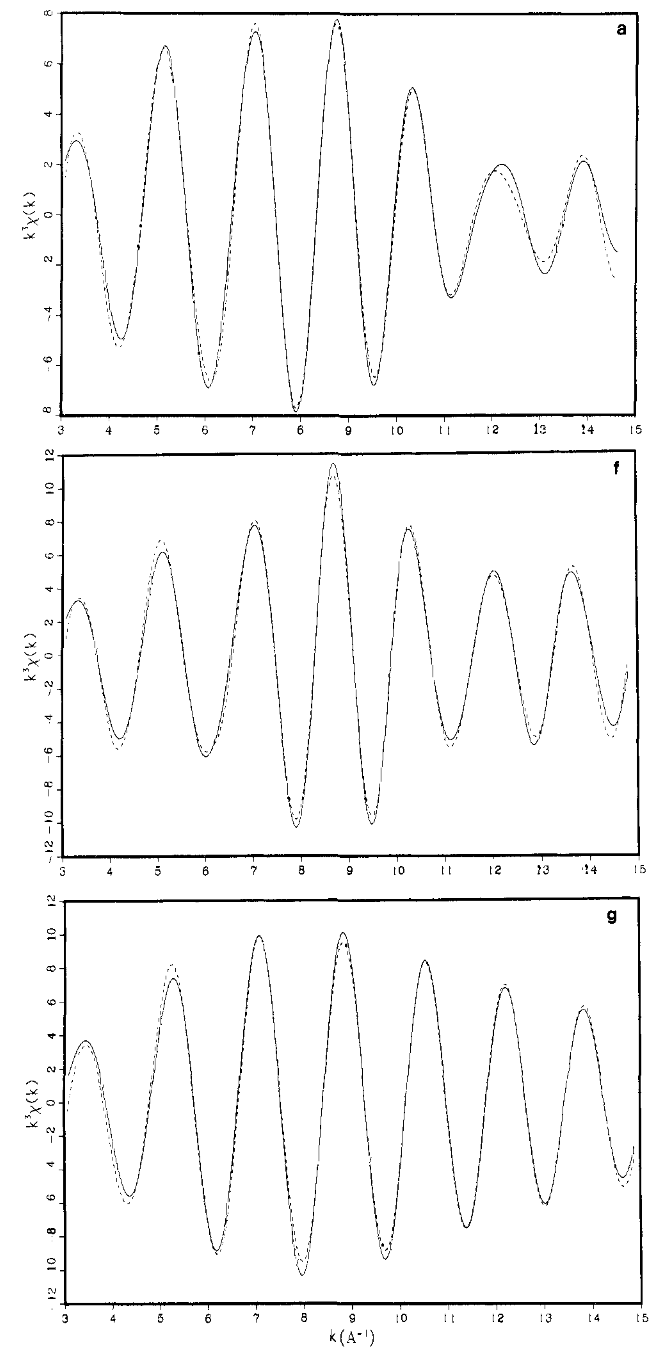

Figure 5. The BFBT nonlinear least-squares curve fit (dashed curve) of the Fourier-filtered $k^3\chi(k)$ vs. k EXAFS spectrum (solid curve) for **1** (a), **6** (f), **7** (g). See supplementary material for the corresponding fits of **2**–**5**.

The resulting least-squares refined interatomic distances, Debye-Waller factors, and coordination numbers (all with estimated standard deviations), as well as energy threshold differences and scale factors, appear in Table I. We shall refer to these results as best fits based on theory (BFBT); they are model independent. Also included in Table I are "best fit" results with the ratio of the scale factors for the two terms (Mo–Fe/Mo–S) fixed at the known values of 1/4 for **1**–**5** and 1/2 for **6**.

The E_0 Problem and the Edge Position. Since the phase functions are unique only when a particular energy threshold, E_0, is specified, our somewhat arbitrary choice of E_0^{exp} = 19 980 eV

(34) Teo, B.-K., to be submitted for publication.

Table I. Best Fit (Based on Theoretical Functions) Least-Squares Refined Interatomic Distances r (Å), Debye-Waller Factors σ (Å), and Coordination Numbers (N) with Standard Deviations (in Parentheses), along with Energy Threshold Differences $\Delta E_0{}^{p}$ (eV) and Scale Factors (B). Also Included are the Edge Position Energies $E_0{}^{p}$ (eV) and a Comparison of the EXAFS Results with Those Obtained from Single-Crystal X-ray Diffraction Studies

		DISTANCE					COORDINATION NUMBER			
		EXAFS			DIFFRACTION[a]		EXAFS			
Cmpd.	Term	E_0^p	ΔE_0^p	r	r	% error	σ	B	N[b]	% error
1	Mo-S	19985	5.43	2.223(12)	2.204(3)	0.9	0.067(9)	2.544	4.9(7)	22.3
			5.79[c]	2.225[c]			0.068[c]	2.586[c]	5.0[c]	25.2[c]
	Mo-Fe	19985	-15.57	2.724(29)	2.756(1)	-1.2	0.000(46)	0.226	0.3(1)	-71.1
			-8.84[c]	2.745[c]			0.069[c]	0.646[c]	1.3[c]	26.2[c]
2	Mo-S	19983	4.55	2.214(18)	-	-	0.060(15)	2.120	3.9(9)	-3.1
			4.44	2.213			0.059	2.094	3.8	-5.1
	Mo-Fe	19983	-4.68	2.789(64)	2.786(1)	0.1	0.055(42)	0.390	0.7(6)	-31.2
			-4.90	2.789			0.066	0.523	1.0	-0.1
3	Mo-S	19984	6.82	2.217(11)	2.199(6)	0.8	0.062(9)	2.534	4.7(6)	17.3
			6.82	2.217			0.063	2.554	4.8	19.2
	Mo-Fe	19984	-14.17	2.739(43)	2.797(9)	-2.1	0.051(39)	0.312	0.6(4)	-39.5
			-12.65	2.745			0.080	0.638	1.4	36.1
4	Mo-S	19982	6.65	2.225(10)	2.203(3)	1.0	0.056(8)	2.313	4.1(5)	2.7
			6.26	2.224			0.057	2.347	4.2	4.9
	Mo-Fe	19982	-15.62	2.736(45)	2.778(5)	-1.5	0.049(39)	0.268	0.5(3)	-54.6
			-18.15	2.726			0.082	0.587	1.3	27.2
5	Mo-S	19982	6.72	2.226(11)	2.213(7)	0.6	0.061(9)	2.211	4.1(6)	1.8
			6.67	2.226			0.061	2.223	4.1	2.3
	Mo-Fe	19982	-1.45	2.752(72)	2.740(1)	0.4	0.044(43)	0.188	0.3(2)	-69.2
			11.37	2.809			0.090	0.556	1.3	29.3
6	Mo-S	19984	7.20	2.237(9)	2.204(5)	1.5	0.043(10)	2.313	3.8(5)	-5.8
			7.16	2.237			0.043	2.292	3.7	-6.7
	Mo-Fe	19984	-4.00	2.769(35)	2.775(6)	-.2	0.065(23)	0.810	1.5(7)	-23.3
			-3.84	2.770			0.078	1.146	2.4	20.1
7	Mo-S	19984	8.35	2.206(8)	2.17(1)	1.2	0.041(11)	2.509	4.0(6)	0.8

[a] The single-crystal X-ray diffraction data were obtained from ref 18a for 1 and 2, ref 18c for 3 and 4, and ref 19b, 19c, and 39 for 5, 6, and 7, respectively. Average interatomic distances are listed for all Mo–S terms and for the Mo–Fe term in 6. [b] Obtained by dividing the scale factors by empirically determined amplitude reduction factors, $S = 0.782(1 - 5\sigma)$, as per eq 2. [c] Throughout this table, the parameters in the second lines within each term were obtained from the curve fitting with the known ratio of Mo–Fe/Mo–S interactions fixed, i.e., $B_{Fe}/B_S = 0.25$ for 1–5, and 0.5 for 6.

may not be consistent with the theoretical E_0's for each of the different types of neighbors for which the theoretical phase shifts are defined.[15b] We must therefore allow a different E_0 value for each type of neighboring atom.[17,29] In practice, we least-squares refine

$$\Delta E_{0j} = E_{0j}{}^{th} - E_0{}^{exp} \tag{4}$$

in

$$k_j = \sqrt{k^2 - 2(\Delta E_{0j})/7.62} \tag{5}$$

where k is the "experimental" wave vector with "experimental" threshold energy $E_0{}^{exp}$ and k_j is the "theoretical" wave vector with the "theoretical" threshold energy $E_{0j}{}^{th}$ associated with atom j.

Our experience shows that, in the curve-fitting process, parameter correlation between a given ΔE_0 and r can occur and, in some cases, can cause errors of up to 0.10 Å. Lowering the value of ΔE_0 tends to shorten the distance and vice versa. Changing ΔE_0 by ca. 1–3 eV often causes a change of ca. 0.01 Å in the distance. In the next section we will describe a "fine-adjustment" method that alleviates to a large extent this correlation, thereby improving the accuracy of distance determination to better than or about 0.01 Å.

Since ΔE_0 depends on $E_0{}^{exp}$, it is desirable to standardize the choice of E_0 such that ΔE_0 obtained from different runs can be compared. In this paper, we choose to use the "edge position", $E_0{}^{p}$, defined as the photon energy taken at half-height of the "edge jump", as the reference point for the energy. The edge jump, $\Delta\mu X$, which is used in the normalization of the data, is the step at the absorption edge measured by extrapolating the EXAFS region to the edge (viz., ignoring the "white lines", if any). Figure 6 shows the edge region of the data in energy space of **5**, from which the edge position of 19 982 eV can be determined. Table I contains the edge positions for compounds **1–7**.

With reference to the edge position, $E_0{}^{p}$, the standardized ΔE_0, $\Delta E_0{}^{p}$, can be defined as

$$\Delta E_{0j}{}^{p} = E_{0j}{}^{th} - E_0{}^{p} \tag{6}$$

Substituting for $E_{0j}{}^{th}$ from eq 4 into eq 6, we have

$$\Delta E_{0j}{}^{p} = \Delta E_{0j} + E_0{}^{exp} - E_0{}^{p} \tag{7}$$

where $E_0{}^{exp}$ was chosen above the absorption edge and ΔE_{0j} was obtained from curve fitting of the k-space data based on $E_0{}^{exp}$ (vide

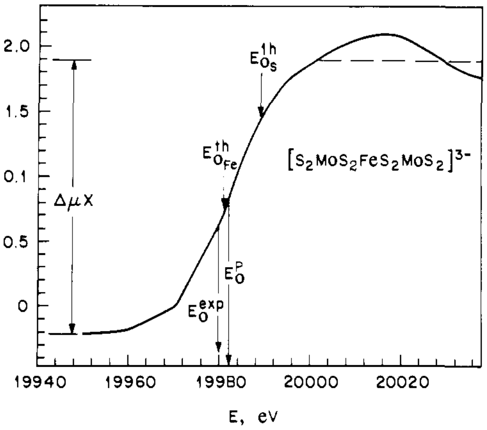

Figure 6. The X-ray absorption near edge region (10-eV steps below the edge) for $[S_2MoS_2FeS_2MoS_2]^{3-}$ (**5**), showing the edge jump ($\Delta\mu X$), the experimental choice for the energy threshold (E_0^{exp}), the energy of the edge position (E_0^{P}), and the values of the BFBT refined edge energies for S (ΔE_{0S}^{th}) and Fe (ΔE_{0Fe}^{th}) consistent with the theoretical phase functions.

infra). As we shall see later, ΔE_0^{P} is related to the difference between the atomic model[17] and the realistic molecular environment sensed by the photoelectron in the EXAFS phenomenon.

With the exception of the definition of the edge position, the data-analysis technique described thus far follows closely the method developed in our previous publications.[1e,f,5,29,35] As can be seen from Table I, the accuracies for both BFBT distance (r) and coordination number (N) determinations are 1% (~0.03 Å) and 20%, respectively, for Mo–S bonds and 2% (~0.06 Å) and 40%, respectively, for Mo–Fe distances. A significant part of these errors is believed to be caused by, in addition to experimental errors and approximations inherent in the EXAFS model[32,33,36] (eq 1), parameter correlation in the nonlinear least-squares curve fitting,[37,38] especially between parameters ΔE_0 and r, and parameters σ and B or N within each term.

Fine Adjustment Based on Model Compounds (FABM). Most of these correlation problems can be removed by restricting ΔE_0^{P} and σ in the curve-fitting process to predetermined values, such as those obtained from analyzing model compounds measured under similar experimental conditions. Alternatively, a fine adjustment technique based on model(s) (FABM) can be applied to the best fit parameters resulting in an improvement of the accuracy. It should be emphasized that the EXAFS parameters (r and N) obtained in the FABM approach are dependent on the model compound(s) employed, whereas the parameters (r, σ, and N) obtained in the initial best fitting with theoretical amplitude and phase functions (BFBT) are model independent.

In the FABM approach, one must measure and analyze the EXAFS of one or more model compounds which, when taken together, contain the same set of neighboring atoms as might be anticipated in the local structural environment around the absorber in the unknown. The model compounds need not encompass all types or numbers of the neighboring atoms in the unknown, but each different absorber–backscatterer pair in the "core" structure of the unknown requires at least one model compound. In order to achieve high accuracy, it is important that the experimental conditions, such as beam line harmonics and the mode of data acquisition (i.e., transmission or fluorescence), be essentially identical for both model and unknown.

(35) (a) Teo, B.-K.; Lee, P. A.; Simons, A. L.; Eisenberger, P.; Kincaid, B. M. *J. Am. Chem. Soc.* **1977**, *99*, 3854. (b) Lee, P. A.; Teo, B.-K.; Simons, A. L. *Ibid.* **1977**, *99*, 3856. (c) Teo, B. K.; Kijima, K.; Bau, R. *Ibid.* **1978**, *100*, 621. (d) Teo, B.-K.; Eisenberger, P.; Reed, J.; Barton, J. K.; Lippard, S. J. *Ibid.* **1978**, *100*, 3225.

(36) (a) Lengeler, B.; Eisenberger, P. *Phys. Rev. B* **1980**, *21*, 4507. (b) Eisenberger, P.; Lengeler, B. *Ibid.* **1980**, *22*, 3551.

(37) Brown, G. S.; Doniach, S., ref 2c, pp 353–385.

(38) Cramer, S. P. In "Synchrotron Radiation Applied to Biophysical and Biochemical Research"; Castellani, A., Quercia, I. F., Eds.; Plenum Press: New York, 1979; pp 291–322.

Table II. Least-Squares Refined Energy Threshold Differences ΔE_0^{P} (eV) and Debye–Waller Factors σ (Å) Obtained from a Restrictive Curve-Fitting Procedure in Which the Distances and the Ratio of Neighbors, N_{Fe}/N_S, Were Fixed at the Crystallographic Values. Amplitude Reduction Factors Are Included along with Average Values

		DISTANCE	COORDINATION NUMBER	
Cmpd.	Term	ΔE_0^{p} [a]	σ	S* [b]
1	Mo-S	2.00(2.00)	0.066	0.572
	Mo-Fe	-6.52(-5.55)	0.066	0.550
2	Mo-S	-	-	0.534
	Mo-Fe	-5.80(-5.71)	0.066	0.579
3	Mo-S	3.57(3.56)	0.061	0.615
	Mo-Fe	-0.10(0.52)	0.078	0.493
4	Mo-S	2.28(2.27)	0.055	0.621
	Mo-Fe	-7.86(-4.59)	0.079	0.433
5	Mo-S	4.18(4.19)	0.060	0.549
	Mo-Fe	-4.87(-5.67)	0.088	0.357
6	Mo-S	-0.40(-.23)	0.043	0.569
	Mo-Fe	-3.23(-2.84)	0.076	0.509
7	Mo-S	-0.29(-.13)	0.041	0.635
Average Values	Mo-S	1.89(1.94)	0.061[c],0.042[d]	0.585
	Mo-Fe	-4.73(-3.97)	0.076	0.487

[a] The numbers in parentheses were obtained from the regression coefficients listed in Table III and the crystallographically observed distances. Note that the two sets agree to ca. 1 eV except the Mo–Fe term of 4 where a difference of 3 eV is observed. The discrepancy, which amounts to ca. 0.01 Å, is due to "different cross sections" of the multiparameter space in the restricted fit and best fit least-squares refinements. Either set can be used as long as one is consistent. [b] Amplitude reduction factors calculated from the scale factors B_u (cf. Table IV) obtained at the characteristic σ values (i.e., σ_{Mo-S} = 0.061 Å for 1–5 and 0.042 Å for 6 and 7; σ_{Mo-Fe} = 0.076 Å) and the known number of sulfur and iron neighbors, according to eq 2. [c] Average of 1–5. [d] Average of 6 and 7.

Restricted Fits. In order to obtain the "characteristic" ΔE_0^{P} and σ values, the EXAFS of the model compounds is fitted with eq 1. The ratio of the two scale factors (Mo–Fe vs. Mo–S) and the two distances are fixed at the known (crystallographic) values.[18a,c,19b,c,39] From such a "restricted" fit, we obtain two ΔE_0^{P} values (via eq 7), ΔE_{0S}^* and $\Delta E_{0_{Fe}}^*$, two Debye–Waller factors, σ_S^* and σ_{Fe}^*, and two amplitude reduction factors $S_S^* = B_S/N_S$ and $S_{Fe}^* = B_{Fe}/N_{Fe}$. The results are tabulated in Table II. The average characteristic values for ΔE_0^*, σ^*, and S^*, obtained from **1**–**7** are: 1.89 eV, 0.061 Å (excluding **6** and **7**), and 0.585 for Mo–S, and −4.73 eV, 0.076 Å, and 0.487 for Mo–Fe (excluding **7**). As is evident from Table I, compounds **6** and **7** have significantly lower σ values for the Mo–S term than compounds **1–5**, indicating a smaller static disorder (distance spread). The average characteristic σ_S^* for **6** and **7** is 0.042 Å, which provides a measure of the vibrational contribution to the Debye–Waller factor for these systems (vide infra). For single-term systems such as MoS_4^{2-}, only the distance is fixed at the known value.

Restricted fitting will generally lead to poorer quality fits with a larger uncertainty in accuracy than does best fitting. For cases where the restricted fits are unsatisfactory, a more reliable method is to use the parameter correlation curves described in the following sections.

Fine Adjustment of Interatomic Distances. The fine adjustments of the distances involves the transfer of the characteristic ΔE_0^* for each type of backscatterer from the model to the unknown system.

A series of fits are obtained by fixing the distance of interest at different values of up to ±0.10 Å away from the best fit value and allowing both scale factors (B_j) and the remaining parameters within the same term to vary during the least-squares refinement. All parameters associated with the other term, except the scale

(39) Schäfer, H.; Schäfer, G.; Weiss, A. *Z. Naturforsch.* **1964**, *196*, 76.

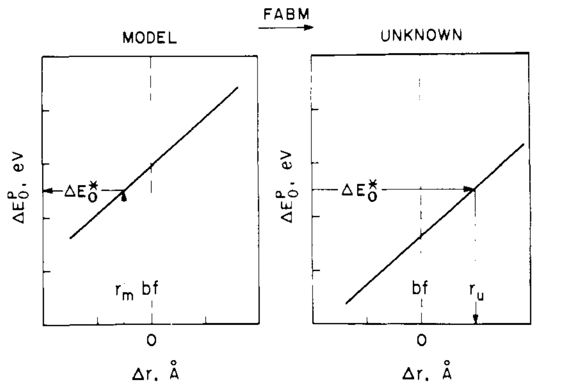

Figure 7. Schematic description of the FABM distance adjustment. At the known crystallographic distance for the model (r_m), a characteristic $\Delta E_0{}^*$ is obtained, which is then transferred to the unknown system to yield the distance adjustment (r_u) to the BFBT ($\Delta r = 0$) refined distance.

Table III. Linear Least-Squares Regression Coefficients[a] for the Two-Term (Linear) $\Delta E_{0j}{}^{p}$ vs. Δr_j Correlation and the Three-Term (Quadratic) B_j vs. σ_j Correlation (j = S and Fe)

		DISTANCE		COORDINATION NUMBER		
Cmpd.	Term	a_0, eV	a_1, eV/Å	b_0[b]	b_1, Å^{-1}	b_2, Å^{-2}
1	Mo-S	5.267	171.878	1.148	1.180	286.899
	Mo-Fe	-15.866	322.404	0.225	0.141	54.418
2	Mo-S	4.509	197.27	1.093	2.104	246.000
	Mo-Fe	-4.989	240.408	0.202	-0.595	73.111
3	Mo-S	6.816	180.679	1.265	1.147	302.687
	Mo-Fe	-14.221	254.185	0.173	-0.373	60.393
4	Mo-S	6.673	200.309	1.322	1.626	285.102
	Mo-Fe	-15.065	249.309	0.156	-0.180	50.272
5	Mo-S	6.657	189.99	1.136	1.231	264.835
	Mo-Fe	-2.081	298.926	0.231	-4.704	83.75
6	Mo-S	7.122	222.809	1.623	1.811	327.440
	Mo-Fe	-4.106	211.670	0.332	-1.498	138.319
7	Mo-S	8.222	232.075	1.804	2.464	357.619

[a] The goodness of fit, R^2, was always greater than 0.998 (with the majority of them better than 0.999) for the data ranges depicted in Figures 8 and 10. [b] Unitless.

factor, are held constant at their best fit values. Thus, the four parameters refined are the Debye–Waller σ and the ΔE_0 of the particular term under consideration, as well as both scale factors. A plot of $\Delta E_0{}^p$ vs. Δr produces the distance correlation curves shown schematically in Figure 7 for model and unknown. It is obvious that as the distance deviates from the best fit value, the goodness of fit deteriorates progressively. The characteristic value $\Delta E_0{}^*$ for the model compound can be determined from the curve at the crystallographic value r_m. The characteristic $\Delta E_0{}^*$ is then transferred to the unknown to determine the distance correction Δr. The "corrected" distance r is given by

$$r = r_{bf} + \Delta r \tag{8}$$

where r_{bf} is the best fit distance.

Since $\Delta E_0{}^p$ vs. Δr plots are normally linear as shown in Figures 8a and 8b for the Mo–S and Mo–Fe terms of **1**–**7**, respectively, it is convenient to least-squares fit the curves with a linear function

$$\Delta E_0{}^p = a_0 + a_1(\Delta r) \tag{9}$$

The intercept a_0 corresponds to the best fit $\Delta E_0{}^p$ (i.e., from BFBT). The slope a_1, normally in the range of 150–320 eV/Å (or 1.5–3.2 eV per 0.01 Å), is the change in threshold energy as a function of distance. The results of these linear regressions (goodness of fit, R^2, ≥0.999) are tabulated in Table III for both Mo–S and Mo–Fe interactions. It is seen that the coefficients a_0 and a_1 vary from term to term (e.g., Mo–S vs. Mo–Fe) and from compound to compound, with relatively large differences between the parameters for different types of scatterers. The distance adjustment

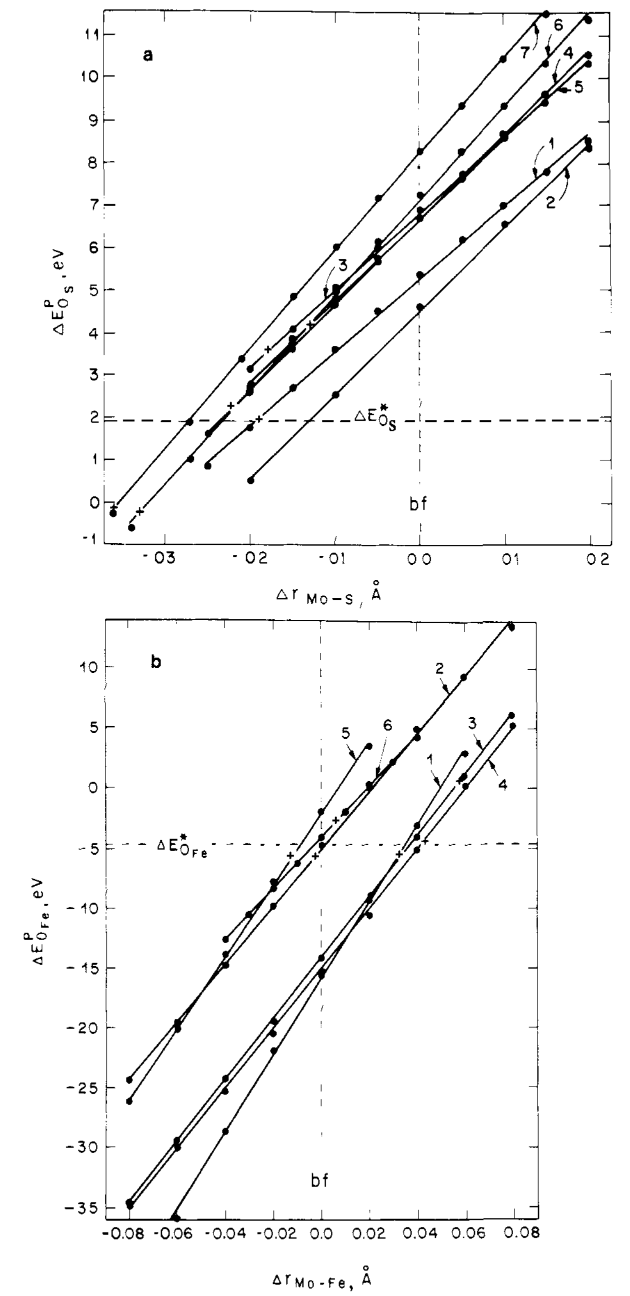

Figure 8. The linear parameter correlation curves $\Delta E_0{}^p$ (eV) vs. Δr (Å) for the (a) Mo–S terms and (b) Mo–Fe terms in compounds **1**–**7**. The crystallographic distances are indicated by + and the average characteristic $\Delta E_0{}^*$ values and the BFBT refined distances (cf. Table I, for which $\Delta r = 0$ herein) are presented as horizontal and vertical dashed lines, respectively.

can then be calculated via $\Delta r = (\Delta E_0{}^* - a_0)/a_1$ where $\Delta E_0{}^*$ is the characteristic value of $\Delta E_0{}^p$ for the particular term. The results are tabulated in Table IV for Mo–S and Mo–Fe distances.

Three points of caution must be made. First, the goodness of fit R^2 must be greater than 0.998 to justify using the linear regression. For $\Delta E_0{}^p$ vs. Δr plots with some curvature, the actual curves (i.e., the graphical method described in Figure 7) should be used. Second, the range in Δr must include both the characteristic $\Delta E_0{}^*$ and the best fit $\Delta E_0{}^p$. Third, though it is equally viable to hold $\Delta E_0{}^p$ rather than r at values away from the best fit value in the series of fits, our experience shows that the resulting $\Delta E_0{}^p$ vs. Δr curves are somewhat different for the two approaches because of the different "cross sections" in the χ^2 surface.

Fine Adjustment of Coordination Numbers. A similar procedure can be applied to the fine adjustment of coordination numbers. A series of fits are made by holding the Debye–Waller factor (σ) of one term at different values (on a specified interval) covering

Table IV. Fine Adjustments (Based on Model Compounds) to the BFBT Results (cf. Table I) for Interatomic Distances r (Å) and Coordination Numbers (N) with Standard Deviations[a] (in Parentheses), along with Scale Factors (B) and Comparisons to X-ray Diffraction Results

		DISTANCE			COORDINATION NUMBER		
Cmpd.	Term	Δr[b]	r	% error[c]	B[d]	N[e]	% error
1	Mo-S	-0.021	2.202(12)	-0.1	2.288	3.9(8)	-2.2
	Mo-Fe	0.034	2.758(45)	0.1	0.550	1.1(5)	13.0
2	Mo-S	-0.013	2.201(10)	-	2.137	3.7(7)	-8.7
	Mo-Fe	0.0000	2.789(60)	0.1	0.579	1.2(6)	18.9
3	Mo-S	-0.027	2.190(12)	-0.4	2.461	4.2(9)	5.2
	Mo-Fe	0.037	2.776(57)	-0.7	0.493	1.0(5)	1.3
4	Mo-S	-0.024	2.201(10)	-0.1	2.482	4.2(8)	6.1
	Mo-Fe	0.044	2.780(58)	0.1	0.433	0.9(4)	-11.1
5	Mo-S	-0.025	2.201(11)	-0.5	2.197	3.8(8)	-6.1
	Mo-Fe	-0.011	2.741(52)	0.0	0.357	0.7(4)	-26.7
6	Mo-S	-0.024	2.213(9)	0.4	2.277	3.9(7)	-2.7
	Mo-Fe	-0.003	2.766(68)	-0.3	1.017	2.1(11)	4.5
7	Mo-S	-0.028	2.178(9)	0.4	2.538	4.3(8)	8.5

[a] The overall standard deviations for the FABM distances and coordination number (due to the uncertainties in both the BFBT and FABM treatments) can be calculated as the square root of the sum of squares of the BFBT and FABM deviations. [b] Distance corrections were calculated according to eq 9 with $\Delta E_{0S}^* = 1.89$ eV and $\Delta E_{0Fe}^* = -4.73$ eV, the averaged values from the restrictive fits; cf. Table II. The asterisks designate the characteristic $\Delta E_0^{\,p}$ values. [c] See Table I for the corresponding crystallographic distances. [d] Scale factors were obtained via eq 10 at $\sigma_S^* = 0.061$ Å for 1-5, $\sigma_S^* = 0.042$ Å for 6 and 7, and $\sigma_{Fe}^* = 0.0076$ Å for 1-6. These Debye-Waller factors are the averaged values obtained from restrictive fits; cf. Table II. The asterisks designate the characteristic values of σ. [e] Calculated via $N = B/S^*$ (cf. eq 2) using the average $S^* = 0.585$ for sulfur and the average $S^* = 0.487$ for iron; cf. Table II.

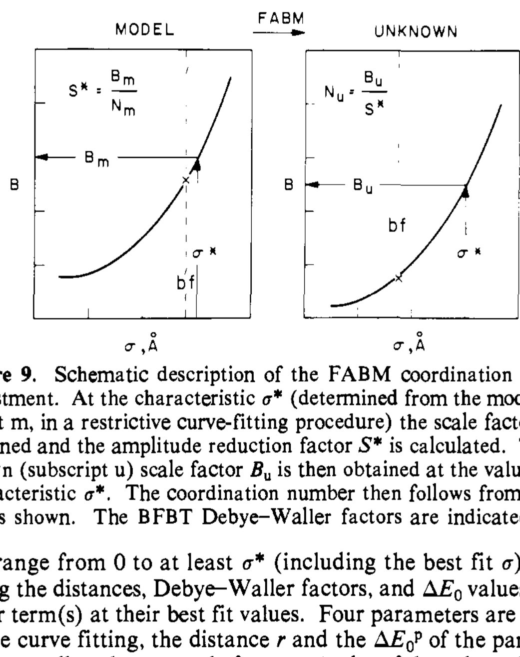

Figure 9. Schematic description of the FABM coordination number adjustment. At the characteristic σ^* (determined from the model, subscript m, in a restrictive curve-fitting procedure) the scale factor B_m is obtained and the amplitude reduction factor S^* is calculated. The unknown (subscript u) scale factor B_u is then obtained at the value of the characteristic σ^*. The coordination number then follows from B_u and S^* as shown. The BFBT Debye-Waller factors are indicated by ×.

the range from 0 to at least σ^* (including the best fit σ), while fixing the distances, Debye-Waller factors, and ΔE_0 values of the other term(s) at their best fit values. Four parameters are refined in the curve fitting, the distance r and the $\Delta E_0^{\,p}$ of the particular term as well as the two scale factors. A plot of the values obtained for B vs. σ will then allow the determination of the B value at the characteristic σ^* value, as depicted graphically in Figure 9. It is obvious that as σ deviates from the best fit value, the goodness of fit deteriorates progressively. An alternative method is to least-squares fit the B vs. σ curve with a quadratic equation

$$B = b_0 + b_1\sigma + b_2\sigma^2 \qquad (10)$$

where the intercept b_0 is the B value at $\sigma = 0$. The pertinent coefficients obtained from the regressions with $R^2 \geq 0.998$ for **1**-**7** are tabulated in Table III. The curves described by the

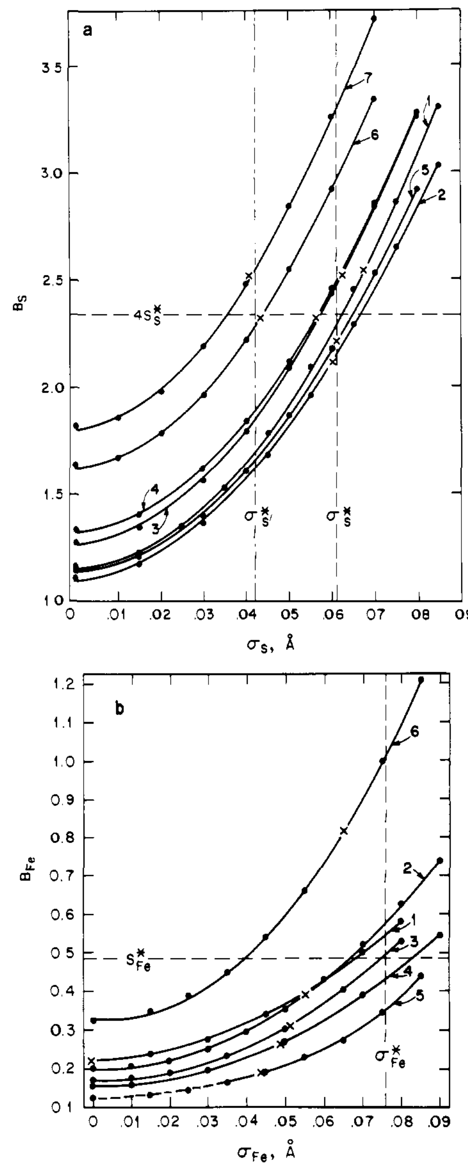

Figure 10. The quadratic parameter correlation curves B vs. σ (Å) for the (a) Mo-S terms and (b) Mo-Fe terms in compounds **1**-**7**. The BFBT Debye-Waller factors are indicated by × and the amplitude reduction factors S^* are shown as horizontal dashed lines. The characteristic σ_S^* = 0.061 Å (**1**-**5**), $\sigma_{S'}^*$ = 0.042 Å (**6**, **7**), and σ_{Fe}^* = 0.076 Å (**1**-**6**) are drawn in with vertical dashed lines.

regression coefficients b_0, b_1, and b_2 in Table III are shown in Figure 10. The same criteria and precautions as described for the distance adjustment hold for the coordination number determination. B can then be calculated from eq 10 for any value of σ within the fitted range.

For each type of neighbor (S and Fe) in the model compounds **1**-**7** (denoted by subscript m), the S^* value at the characteristic σ^* can be obtained from the known coordination number N_m and the value of B_m at σ^*, $S^* = B_m/N_m$ (cf. eq 2). S^* can then be transferred to the unknown systems (denoted by subscript u) in order to calculate the coordination number N, $N_u = B_u/S^*$, where B_u is the value for the unknown obtained at σ^*. The B values at the characteristic σ^* values (σ^* = 0.042 Å for Mo-S in MoS_4^{2-} and **6**, and σ^* = 0.061 Å for Mo-S in **1**-**5** and 0.076 Å for all Mo-Fe) and the predicted N (based on the average S^* = 0.585 for Mo-S and 0.487 for all Mo-Fe) are tabulated in Table IV for both Mo-S and Mo-Fe interactions.

Debye-Waller Factors. Since the fine adjustment technique described in the previous section calls for the determination of a characteristic Debye-Waller factor σ^* from model compounds, it is important to consider the effect of the choice of σ^* on the determination of the number of neighboring atoms. As long as

Table V. Average Molybdenum-Sulfur Terminal and Bridging Interatomic Distances (Å) as Estimated from the EXAFS Determined Debye-Waller Factors (Å), along with Comparisons to the X-ray Crystallographic Data, Where Available

	EXAFS						DIFFRACTION[g]			
Cmpd	σ_{bf}^a	σ_{stat}^b	δr^c	r^d	r_m	r_n	σ_{calc}^e	σ_{stat}^f	r_b	r_t
1	0.067(9)	0.053	0.107	2.203(12)	2.256	2.150	0.065	0.051	2.255(2)	2.153(2)
2	0.060(15)	0.044	0.089	2.201(10)	2.245	2.157	-	-	-	-
3	0.062(9)	0.047	0.095	2.190(12)	2.237	2.143	0.085	0.074[h]	2.273(9)[h]	2.126(26)[h]
4	0.056(8)	0.038	0.078	2.202(10)	2.240	2.164	0.058	0.041	2.244(6)	2.163(13)
5	0.061(9)	0.045	0.092	2.201(11)	2.246	2.156	0.059	0.043	2.256(5)	2.171(5)
6	0.043(10)	0.013	-	2.213(9)	-	-	0.041	0	2.204(5)	-
7	0.041(11)	-	-	2.178(9)	-	-	0.041	0	-	2.18(1)

[a] The least-squares refined BFBT Debye-Waller factors with estimated standard deviations; cf. Table I. [b] The static contribution to the Debye-Waller was calculated using eq 13 and assuming $\sigma_{vib} = 0.041$ Å. [c] Distance spread obtained via eq 12. [d] The average Mo-S interatomic distances from the FABM treatment; (cf. Table IV) with standard deviations. [e] Calculated according to eq 13, assuming $\sigma_{vib} = 0.041$ Å and using the values of σ_{stat} as obtained from the diffraction data[f] (cf. column 8). [f] Calculated from the average crystallographic interatomic distances[g] r_b and r_t using eq 12. [g] The single-crystal X-ray diffraction data are obtained from ref 18a for 1 and 2, ref 18c for 3 and 4, and ref 19b, 19c, and 39 for 5, 6, and 7, respectively. [h] Based on preliminary crystallographic results (ref 18c).

σ^* is consistently chosen and applied to both the unknown and the model systems, it has little effect on the determination of coordination number (vide infra). In this paper, we use the restricted fit (with distances and the scale factor ratio fixed at known values) to determine σ^*. For the major term (Mo–S), it is evident from Tables I and II that the best fit and the restricted fit, respectively, give rise to similar Debye–Waller factors. These values are also quite reasonable from a structural standpoint. However, in the case of the minor term (Mo–Fe), the restricted and best fit values for σ_{Fe} disagree somewhat (cf. Tables I and II), and the σ^* values from the restricted fits were used.

Another way of arriving at characteristic σ^* values is to calculate them from the known structural and spectroscopic data of the model compounds. This also provides a check for the Debye–Waller factors determined experimentally by EXAFS. The calculated values of σ for Mo–S are presented in Table V along with the values obtained by EXAFS spectroscopy; the two sets (σ_{bf} and σ_{calcd}) of Debye–Waller factors are in excellent agreement. The vibrational contribution to the Debye–Waller factor σ_{vib} can be calculated in a diatomic approximation. Using the vibrational frequency of $\bar{\nu} = 475$ cm^{-1} and $K = 2.84$ mdynes/Å[40a] (for MoS_4^{2-}) and the following equation,[41]

$$\sigma_{vib} = 3.151 \times 10^{-3}[(\bar{\nu}/K) \coth (y/2)]^{1/2} \tag{11}$$

where $y = 1.441(\bar{\nu}/T)$, and T is the temperature in K, we obtain $\sigma_{vib} = 0.0451$ Å for the Mo–S bonds in MoS_4^{2-} at room temperature. This is in good agreement with the value of 0.0427 Å, calculated in a more exact treatment by Müller and Nagarajan,[40b] which is also in line with our EXAFS result of 0.041 Å, for **7**. We can then apply this last value of σ_{vib} to calculate the distance spread for all Mo–S bonds in compounds **1–7**; cf. Table V.

The static contribution to the Debye–Waller factor can be estimated by[29a]

$$\sigma_{stat} = \frac{\sqrt{mn}}{m+n}\delta r \tag{12}$$

for m and n bonds of the same type, but differing slightly in distance by δr ($\lesssim 0.1$ Å). The overall Debye–Waller factor is then[29a]

$$\sigma = \sqrt{\sigma_{vib}^2 + \sigma_{stat}^2} \tag{13}$$

Using eq 11–13, one can calculate σ_{calcd} from the known spectroscopic and structural information. For example, in $[S_2MoS_2Fe(SPh)_2]^{2-}$ (**1**), there are two terminal (r_t) and two bridging (r_b) Mo–S bonds at 2.153 (6) and 2.255 (6) Å,[18a] respectively, giving rise to $m = n = 2$ and $\delta r = 0.102$ Å. Using eq 12, $\sigma_{stat} = 0.051$ Å, and assuming $\sigma_{vib} = 0.041$ Å (eq 11), $\sigma = 0.065$ Å can be calculated from eq 13, in good agreement with the value of 0.067 Å determined by EXAFS (cf. Table V). Conversely, one can determine the static contribution to the Debye–Waller factor, σ_{stat}, using eq 13 in which a reasonable σ_{vib} (such as that calculated with eq 11) is assumed. From σ_{stat}, the spread of distances, δr, can be calculated via eq 12 for a known ratio of $m{:}n$. Combining δr and the average distance, r, the two sets of distances, r_m and r_n, can be determined. The results are also tabulated in Table V (cf. second to fifth column). Note that r_m and r_n are in excellent agreement with the crystallographic values, r_b and r_t. With these approximations, the sign of δr cannot be determined and hence the assignment of the two sets of distances to bridging vs. terminal bonds cannot be made.

It is clear from the above discussion that the characteristic σ^* for **6** or **7** should be different from the corresponding value for **1** to **5**. It is gratifying to note from Tables I and II that there are two types of compounds involving MoS_4 units with significantly different Debye–Waller factors: ca. 0.042 Å for **6** and **7** on the one hand, and ca. 0.061 Å for **1–5**, on the other.

Results and Discussion

The average Mo–S and Mo–Fe distances as well as the corresponding S and Fe coordination numbers for compounds **1–7** are tabulated in Tables I (BFBT results) and IV (FABM results). This series of Mo–Fe–S clusters containing the "linear" MoS_2Fe core is of particular importance for several reasons. First, since all of them have been structurally characterized by single–crystal X-ray diffraction techniques, the accuracy of the EXAFS structural determinations can be checked. Second, this series of compounds contains from zero to two iron atoms per molybdenum atom. As such, they might serve as models for the Mo K-edge EXAFS of nitrogenase, which has been shown to be consistent with two to three iron atoms neighboring each molybdenum.[3a–c,5] In the following sections, we shall first compare our EXAFS results based on theory (BFBT) with the crystallographic values (cf. Table I). Then we shall discuss the improvement of the accuracy based on the fine adjustment technique, which is model dependent (FABM; cf. Table IV), with a cautionary note on the criteria for choosing a good model.

Determination of Interatomic Distances. As is evident from Table I, the accuracy of Mo–S and Mo–Fe distances obtained via best fits based on theory (BFBT) amounts to ca. 1 and 2% for the Mo–S and Mo–Fe distances, respectively. As is apparent in the ΔE_0^p vs. Δr correlation curves shown in Figure 8, the characteristic ΔE_0^* obtained at the known crystallographic Mo–S and Mo–Fe distances (indicated by +) are relatively constant for each term, clustering around an average of 1.89 and −4.73 eV (with a spread of 4 and 8 eV) for the Mo–S and Mo–Fe distances, respectively. The distance correction Δr can be calculated either from the characteristic ΔE_0^*, the slope (a_1) of the correlation, and the intercept (a_0) via eq 9 or from the correlation curve, ΔE_0^p vs. Δr, shown in Figures 8a and 8b via the graphical method illustrated schematically in Figure 7. The corrected distances are also listed in Table IV. The accuracy is considerably improved in this FABM treatment of interatomic distances, to better than 0.5 and 1% for Mo–S and Mo–Fe terms, respectively.

Determination of Coordination Numbers. The best fit results for the coordination numbers N_{bf} can be obtained by dividing the best fit scale factors B_{bf} (at σ_{bf}) by approximate amplitude reduction factors,[34]

$$S = s_0^2(1 - 5\sigma) \tag{14}$$

(40) (a) Müller, A.; Weinstock, N.; Mohan, N.; Schläpfer, C. W.; Nakamoto, K. *Appl. Spectrosc.* **1973**, *27*, 257. (b) Müller, A.; Nagarajan, G. *Z. Naturforsch. Teil B* **1966**, *21*, 508.
(41) Cyvin, S. J. "Molecular Vibrations and Mean Square Amplitudes", Elsevier: Amsterdam, 1968; p 71.

Here s_0^2 is the absorbing atom overlap factor, which is 0.782 for molybdenum.[32] Note that eq 14 is not valid for very large Debye–Waller factors, $\sigma \gtrsim 0.1$ Å. The results are tabulated in Table I for best fit based on theory and best fit with the ratio of the scale factors (Mo–Fe vs. Mo–S) fixed at the known ratios. The latter apparently gives better accuracy (ca. 20 and 30%) for the Mo–S and the Mo–Fe terms, respectively.

For fine adjustment (FABM), two amplitude reduction factors, S_S^* and S_{Fe}^*, each obtained at the characteristic Debye–Waller factors, σ_S^* and σ_{Fe}^*, are needed. Figures 10a and 10b illustrate the B vs. σ correlation for the Mo–S and Mo–Fe terms, respectively. The curves shown were drawn from the regression coefficients obtained from the linear least-squares fit (cf. eq 10). The best fit Debye–Waller factors are indicated by crosses, (×), on the graphs. It is obvious from Figure 10 as well as from Table II that the B_S vs. σ_S curves segregate into two sets: for **6** and **7**, $\sigma_S \approx 0.042$ Å, and for **1–5**, $\sigma_S = 0.061$ Å, implying different sulfur environments around molybdenum. Indeed, there are four equivalent Mo–S bonds in **6** and **7**, and two terminal and two bridging Mo–S bonds in **1–5**, as shown in Figure 1. The B_{Fe} vs. σ_{Fe} curves, Figure 10b, for **1** to **6** follow the trend of $N_{Fe} = 1$ (**1–5**), and $N_{Fe} = 2$ (**6**) in order.

Following the method described in a previous section, we obtain the characteristic S^* for Mo–S of 0.585 for compounds **1–7**. The characteristic σ^* are 0.061 Å for **1–5** and 0.042 Å for **6** and **7**. Similarly for Mo–Fe, S^* is equal to 0.487 with a σ^* of 0.076 Å. Using these characteristic values, N_S and N_{Fe} can be calculated via eq 2. The results are listed in Table IV. It is apparent that FABM improves the accuracy of coordination number determination to ±10 and ±20% for the number of sulfur and iron nearest neighbors.

Thickness Effect. To correct for the thickness effect, we used the method developed by Stern and Kim.[42a] The amplitude reduction, $T = \chi'/\chi$, due to the thickness effect, for an edge jump of $\mu_T X$ and a leakage of α, is given by eq 5 in Stern's paper. For BFBT, the thickness effect corrected coordination numbers are $N_{corr} = N_{BFBT}/T$, whereas for FABM,

$$N_{corr} = N_{FABM}(T_m/T_u) \qquad (15)$$

where T_m and T_u are the amplitude reduction factors for the model and unknown, respectively. After thickness correction with a 3% leakage, a slight overall improvement in the accuracy of the sulfur coordination was observed for **1–5** and only minor changes were obtained for the determination of iron nearest neighbors in compounds **1–6**. Other leakage values give rise to no further improvements. The Mo–S corrections calculated for **6** and **7** appear to be in the wrong directions. The problem here may be that α is not constant for pellets of different thicknesses, X, made from powdered samples. In this regard, it is important that measurements be made on thin homogeneous pellets to minimize the thickness effect.

Debye–Waller Factors and the Distance Spreads. Though EXAFS gives only average distances, individual distances (e.g., terminal vs. bridging) can be determined from the Debye–Waller factors. Using either the restricted or the best fit σ and σ_{vib} calculated from vibrational data (cf. eq 11), σ_{stat} can be estimated via eq 13. Then assuming reasonable m and n values, $\delta r = |r_m - r_n|$ can be calculated from eq 12. For $[MoS_4]^{2-}$ and $[Cl_2FeS_2MoS_2FeCl_2]^{2-}$ $\sigma_{stat} \approx 0$ and hence $\delta r = 0$. For **1–5**, $m = n = 2$ and the calculated bridging and terminal Mo–S distances are tabulated and compared with the crystallographic values in Table V.

Crystal Disorder. One advantage of EXAFS spectroscopy is its capability of determining the local structure around an X-ray absorbing atom regardless of the physical state of the sample. A case in point is the $[S_2MoS_2FeCl_2]^{2-}$ dianion **2**, which is crystallographically disordered in all salts examined. Single-crystal X-ray diffraction methods showed that the dianion is twofold disordered about a pseudo-inversion center $\bar{1}$ located halfway between the two metal atoms.[18a,20a] Hence only the average M–S (bridging) and M–X (terminal) distances can be determined crystallographically, where M represents an equal admixture of Mo and Fe, and X an equal admixture of S and Cl. With EXAFS, the Mo–S and Fe–X distances can be determined from the Mo and Fe spectra, respectively. Together with the Debye–Waller factors, we can resolve these average distances into individual terminal vs. bridging bond lengths. Thus, assuming $\sigma_{vib} = 0.041$ Å for the Mo–S bonds in this dianion, the static contribution to the Debye–Waller factor can be calculated from $\sigma_{stat} = (\sigma_{bf}^2 - \sigma_{vib}^2)^{1/2}$. For **2**, $\sigma_{stat} = 0.044$ Å, and using eq 12 we obtain $\delta r = 0.088$ Å, assuming $m = n = 2$. Assuming that the bridging Mo–S distances are longer than the terminal ones, and using the EXAFS determined average Mo–S distance of 2.201 Å, we obtain an average bridging Mo–S distance of 2.245 Å and an average terminal Mo–S distance of 2.157 Å. A similar treatment, when applied to the Fe edge EXAFS of **2** (reported elsewhere),[43] with $\sigma_{vib} = 0.043$ Å (assumed), gives rise to $\sigma_{stat} = ((0.051)^2 - (0.043)^2)^{1/2} = 0.027$ Å, and $\delta r = 0.055$ Å. Using the average Fe–X distance of 2.277 Å, we obtain an average bridging Fe–S distance of 2.304 Å and an average terminal Fe–Cl distance of 2.250 Å. Here the two Fe–S and the two Fe–Cl backscatterings were treated as four Fe–X distances; the backscattering amplitude and phase functions for X were obtained by a simple point-by-point arithmetic average of the corresponding functions for S and Cl. The average metal–S (bridging) and metal–X (terminal) distances of 2.275 and 2.204 Å, respectively, are in good agreement with the corresponding values of 2.263 (2) and 2.200 (2) Å obtained by X-ray crystallography for the twofold disordered dianion.[18a] Using both the EXAFS bridging M–S distances and the Mo–Fe distance (2.786 Å) for **2**, the calculated Mo–S*–Fe bond angle is 75.5°; the crystallographically determined bond angles are 76.00 (5)° [18a] for **2**, 75.18 (6)° [18a] for **1**, and 76.1 (1)° [19c] for **6**. The molybdenum and iron strutural parameters for **2** are thus virtually identical with the corresponding Mo and Fe sites in structures **1** and **6**, respectively.

Criteria for the Selection of Good Model Compounds. It should be emphasized that best fitting based upon theory requires no models, whereas the fine adjustment based upon models method is model dependent. *Hence the FABM distance corrections and coordination number determinations can improve upon the BFBT results if and only if good model compounds are used.* To our knowledge, no simple method is yet available that will enable one to decide whether a model compound is appropriate for an unknown system. Since most EXAFS data-analysis techniques are model dependent, it is desirable to find a way to distinguish a "good" model from a "bad" model. The parameter correlations obtained in our fine adjustment method provide a convenient way for such a differentiation. The following criteria have been developed for choosing an appropriate model compound as well as for applying the FABM method. We note that Bunker et al. have recently reported criteria for a good standard and have also indicated that a good standard is critical to assure the accuracy of the structural parameters.[44]

First, consider the ΔE_0^p vs. Δr plot. As shown schematically in Figure 11, model 1 is a good model for the unknown system because the two curves are nearly parallel, and the resulting distance correction Δr (r_{u1}) is within 0.1 Å. Model 2, however, has a significantly different slope and Δr (r_{u2}) for the unknown is greater than 0.1 Å. Here $\Delta r = 0$ corresponds to the best fit distances, and the fits at the crystallographic distances are indicated as r_{m1}, ΔE_{0m1}^*, and r_{m2}, ΔE_{0m2}^* for models 1 and 2, respectively. The criteria for the ΔE_0^p vs. Δr plots are: (1) the two slopes (a_1 in the regression eq 9) must be similar; and (2) the resulting correction in distance Δr for the unknown must be within ±0.1 Å of the best fit value. For this range the ΔE_0^p vs. Δr plots are usually linear. The criterion of $\Delta r = \pm 0.1$ Å is based on our

(42) (a) Stern, E. A.; Kim, K. *Phys. Rev. B* **1981**, *23*, 3781. (b) An alternate correction for the effects of X-ray leakage is given by: Goulon, J.; Goulon-Ginet, C.; Cortes, R.; Dubois, J. M. *J. Phys. (Paris)* **1982**, *43*, 539.

(43) Antonio, M. R.; Teo, B.-K.; Averill, B. A., submitted for publication.

(44) Bunker, G.; Stern, E. A.; Blankenship, R. E.; Parson, W. W. *Biophys. J.* **1982**, *37*, 539.

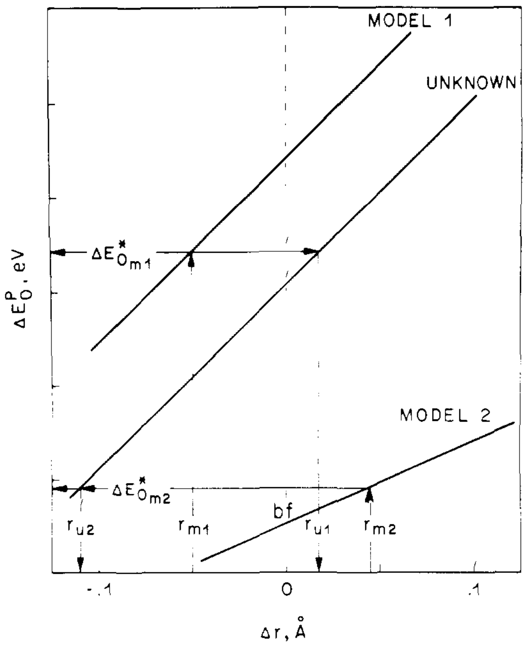

Figure 11. Schematic showing different choices of a model for the distance adjustment in the FABM method. Model 1 is a good model for the unknown because the lines are nearly parallel and the resulting distance correction r_{u1}, obtained at the characteristic $\Delta E_{0_{m1}}*$, is within 0.1 Å of the BFBT unknown distance. Model 2 is a bad model for the unknown because the slopes are not similar and the distance correction r_{u2}, obtained at the characteristic $\Delta E_{0_{m2}}*$, is greater than 0.1 Å.

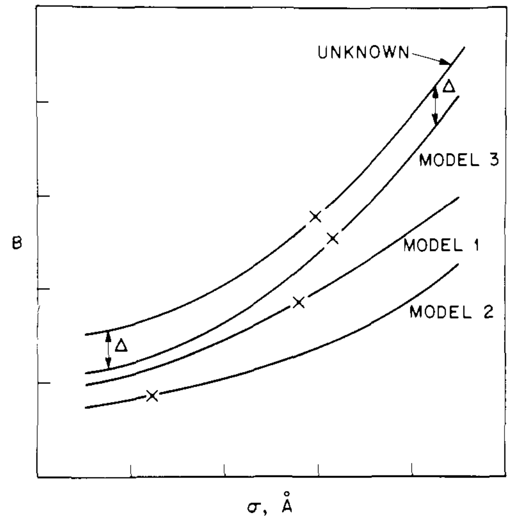

Figure 12. Schematic showing the different choices of a model for coordination number determinations in the FABM method. Model 1 is a good model because the BFBT Debye-Waller factor (indicated by ×) is similar to that of the unknown, and also the ratio of the B values is constant over all σ. Model 2 is inappropriate since it has a BFBT σ significantly different from the unknown. Model 3 is also a bad model because the ratio of the B values (here displaced by a constant difference, Δ) is not independent of σ.

experience that theory alone can predict distances to better than ±0.06 Å. In cases where the two lines are not parallel, Δr values in excess of ±0.1 Å are often observed. In this situation, the fine adjustment technique is not applicable (neither are most model-dependent data analysis techniques). In other words, for such cases the model is a bad one.

For the B vs. σ plot, we impose the following two criteria: (1) the best fit Debye-Waller factors for the model and the unknown system must be similar; and (2) the ratio of the B values (B_{unknown} to B_{model}) for the two systems must be independent of σ (i.e., the ratio should be constant over all σ). In other words, the FABM coordination number, which is calculated from the value of B_u at σ^*, should be independent of the choice of σ^*. As illustrated in Figure 12, model 1 is good since it satisfies both criteria. Model 2 is inappropriate since it has a best fit σ (marked by ×) significantly different from that of the unknown (although it satisfies the second criterion). Model 3 is also inadequate because it does not follow the second criterion (although it satisfies the first one). In fact, model 3 is schematically drawn such that the B values are displaced by a *constant difference*, Δ, from the corresponding values of the unknown. The S^* value obtained from model 3 is not strictly transferable to the unknown.

In fact, it is tempting to generalize these criteria to other model-dependent EXAFS data analysis techniques and to point out that it is risky to base the entire analysis on one point in the multidimensional parameter correlation space. For a good model compound, transfer of such parameters as ΔE_0 and σ will probably allow an accurate determination of interatomic distances and coordination numbers. However, unless and until the suitability of the model is ascertained via the parameter correlation method suggested here or by other established criteria,[44] the results remain *model dependent*.

In addition, to achieve the highest accuracy with the FABM method, the unknown and model(s) must be measured and analyzed in a similar fashion. For dilute biological samples, which are usually measured using the fluorescence mode, this means that frozen solutions of the model compounds should be employed. The parameters (r, σ, and ΔE_0) of the model should be similar to that of the unknown. (This is particularly important if the fitting routine leads to more than one best fit minimum for the unknown and/or the model.)

Conclusion

In this paper, we have measured and analyzed the Mo K-edge EXAFS of a series of Mo-Fe-S compounds containing the MoS_4 unit (cf. Figure 1). To improve the accuracy of the *best fit* results *based on theory* (BFBT), we have developed a *fine adjustment* technique *based* on *models* (FABM). With the FABM technique, interatomic distances and coordination numbers can be determined to better than 0.5 and 10% accuracy, respectively, for the majority term (Mo-S) in the EXAFS spectrum. The corresponding accuracies for the minority term (Mo-Fe) are 1 and 20%.

The FABM method has proven to be most successful herein, as well as in our analyses of the Mo and Fe EXAFS of the $[Cl_2FeS_2MoS_2FeCl_2]^{2-}$ dianion[45] and the Fe EXAFS of the $[(p\text{-}CH_3C_6H_4S)_2FeS_2FeS_2MoS_2]^{3-}$ trianion and the $[(C_6H_5O)_2FeS_2MoS_2]^{2-}$ dianion.[18c] In addition to these studies of synthetic clusters, we have successfully applied the FABM method to the three-Fe cluster of *Desulfovibrio gigas* ferredoxin II[46] and the Fe EXAFS of the FeMo cofactor of nitrogenase.[4]

The advantage of the FABM technique lies with the detailed exploration of the multidimensional parameter correlation space. In particular, one can (1) determine error estimates for each parameter; (2) discover and discriminate against false (local) minima, if any, in the curve fitting; and, most importantly, (3) differentiate a good model from a bad one. The prime criterion for a good model is that the χ^2 minimum surface in the parameter correlation space must have *parameters* and *curvature* similar to those of the unknown. While it is almost impossible to explore all the parameters, we have focused our attention on the correlations of the most important ones (ΔE_0^P vs. Δr, and B vs. σ), which correspond to certain cross sections of the multidimensional parameter space. A few simple criteria have been developed that may be used to assess potential model compounds and to improve the accuracy of the EXAFS results.

It should be emphasized that the FABM technique is model dependent. As with any other model-dependent data analysis technique, the results are accurate to the extent that the parameters and parameter correlations for a given model compound mimic those of the unknown system. However, the FABM method is distinct from other model-dependent techniques in that only one

(45) Teo, B.-K.; Antonio, M. R.; Coucouvanis, D.; Simhon, E. D. *J. Am. Chem. Soc.*, accepted for publication.

(46) Antonio, M. R.; Averill, B. A.; Moura, I.; Moura, J. J. G.; Orme-Johnson, W. H.; Teo, B.-K.; Xavier, A. V. *J. Biol. Chem.* **1982**, *257*, 6646.

parameter (ΔE_0^*), *and not the total phase function*, needs to be obtained from the model to calculate the distance in the unknown. Similarly, only two parameters (σ^*, S^*), *and not the complete amplitude function*, need to be obtained from the model to calculate the number of neighbors in the unknown. In the FABM approach, theoretical phase and amplitude functions, rather than functions extracted from models, are used in the curve fitting. In this respect, the method is less critically dependent on the models than other model-based techniques.

Terminal and bridging Mo–S distances can also be determined quite accurately from both the average Mo–S distance and the distance spread estimated from the determined Debye–Waller factor. This technique also allows us to determine the individual terminal Mo–S and Fe–Cl, as well as bridging Mo–S and Fe–S, distances in the twofold disordered anion $[S_2MoS_2FeCl_2]^{2-}$, where only average terminal M–X (M = (Mo + Fe)/2, X = (S + Cl)/2) and average bridging M–S distances can be determined from single-crystal X-ray crystallography.[18a,20a]

Acknowledgment. This research was supported in part by the National Science Foundation (CHE-7715990) and the USDA/SEA Competitive Grants Office (5901-0418-8-0175-0) to B.A.A., and by a Sigma Xi Research Support Grant (M.R.A.). B.A.A. was an Alfred P. Sloan Foundation Fellow, 1981–83. We thank Drs. D. Coucouvanis (University of Iowa), H. C. Silvis, and R. H. Tieckelmann (Michigan State University) for providing the compounds studied herein, and we are also indebted to V. Bakirtzis (Bell Labs) for her valuable assistance. We are grateful to Dr. D. Mills at CHESS for his generous assistance with the EXAFS apparatus and the data acquisition.

Appendix

Error Estimates. The same stepwise curve-fitting procedure involved in the fine adjustment of distances and coordination numbers (see the corresponding previous sections) also yields the estimated standard deviations for these parameters as well as for the Debye–Waller factors. For the series of fits, the chi-square, Σ^2 were plotted vs. the r_j or σ_j parameters. The BFBT standard deviations for r_S and σ_S were obtained as one-half of the total range (in Å), centered around the refined parameter minimum, over which the Σ^2 contribution doubled the minimum Σ^2 value of the best fit. The standard deviations for r_{Fe} and σ_{Fe} were obtained as the range over which the best fit Σ^2 contribution increases by the percentage corresponding to N_{Fe}/N_S (e.g., $N_{Fe}/N_S = 0.25$ or 25% for **1**–**5**, and $N_{Fe}/N_S = 0.5$ or 50% for **6**).

Estimating the BFBT coordination number standard deviations for each term first involves the calculation of B values (B_1 and B_2), according to eq 10, at each extreme of the range in σ, as determined above, around σ_{bf}. Knowing the amplitude reduction factor S calculated at σ_{bf} via eq 14, the quoted standard deviations were obtained in the following manner:

$$(\Delta N)_{BFBT} = \left|\frac{B_1 - B_2}{2S}\right| \quad \text{(A)}$$

Note that the BFBT error estimates in parentheses, (cf. Table I) for r, σ, and N represent the systematic errors associated with the nonlinear least-squares curve fitting only.

The FABM standard deviations for coordination number and distance (cf. Table IV, in parentheses) are systematic errors associated with the transfer of the parameters (ΔE_0^*, σ^*, and S^*) from the model compounds to the unknowns. The deviation in the coordination number originates with the uncertainty in both the B values of the unknown (combined with the error in σ^* for the model) and the model S^* values according to

$$(\Delta N)_{FABM} = \sqrt{(\Delta N_B)^2 + (\Delta N_S)^2} \quad \text{(B)}$$

This equation can be rewritten into a calculable expression

$$(\Delta N)_{FABM} = \left\{\left[\frac{B_{u1} - B_{u2}}{2S^*}\right]^2 + \left[\frac{N_m B_u}{2}\left(\frac{1}{B_{m1}} - \frac{1}{B_{m2}}\right)\right]^2\right\}^{1/2} \quad \text{(C)}$$

The first term is similar to that used in determining the BFBT deviations (cf. eq A). Here B_{u1} and B_{u2} as well as B_{m1} and B_{m2} are calculated at the extrema for the range in σ^* for the unknown and the model, respectively. Finally, B_u is the B value for the unknown at σ^* and N_m is the known number of neighbors for the model.

The FABM distance standard deviation originates with the uncertainty in the value of the characteristic ΔE_0^*. The model compound ΔE_0^p extrema (centered around ΔE_0^*) are obtained from the distance extrema (corresponding to the BFBT distance spread; vide supra) centered around the crystallographic distance. These ΔE_0^p extrema, when transferred to the unknown, define a distance spread; the standard deviation for r is then half of this total range.

Registry No. 1, 72089-28-2; **2**, 74429-28-0; **3**, 79469-83-3; **4**, 83214-37-3; **5**, 75282-37-0; **6**, 73621-80-4; **7**, 15060-55-6; Mo, 7439-98-7.

Supplementary Material Available: Tables of the raw absorption data in the form ln I_0/I vs. E (in eV) for **1**–**7**, Figures 2b–g (ln I_0/I vs. E) and Figures 3b–g (the background subtracted data $k^3\chi(k)$ vs. k, and the Fourier-filtered data $k^3\chi(k)$ vs. k) for **2**–**6**, and Figures 4b–e (Fourier transforms) and Figures 5b–e (best fits) for **2**–**5** (40 pages). Ordering information is given on any current masthead page.